



Morphological Study of the Cortical and Thalamic Glutamatergic Synaptic Inputs of Striatal Parvalbumin Interneurons in Rats

Xuefeng Zheng^{1,2} · Liping Sun³ · Bingbing Liu^{4,6} · Ziyun Huang¹ · Yaofeng Zhu^{1,5} · Tao Chen¹ · Linju Jia¹ · Yanmei Li¹ · Wanlong Lei¹

Received: 29 June 2020 / Revised: 14 February 2021 / Accepted: 17 March 2021 / Published online: 26 March 2021
© The Author(s), under exclusive licence to Springer Science+Business Media, LLC, part of Springer Nature 2021

Abstract

Parvalbumin-immunoreactive (Parv+) interneurons is an important component of striatal GABAergic microcircuits, which receive excitatory inputs from the cortex and thalamus, and then target striatal projection neurons. The present study aimed to examine ultrastructural synaptic connection features of Parv+ neurons with cortical and thalamic input, and striatal projection neurons by using immuno-electron microscopy (immuno-EM) and immunofluorescence techniques. Our results showed that both Parv+ somas and dendrites received numerous asymmetric synaptic inputs, and Parv+ terminals formed symmetric synapses with Parv- somas, dendrites and spine bases. Most interestingly, spine bases targeted by Parv+ terminals simultaneously received excitatory inputs at their heads. Electrical stimulation of the motor cortex (M1) induced higher proportion of striatal Parv+ neurons express c-Jun than stimulation of the parafascicular nucleus (PFN), and indicated that cortical- and thalamic-inputs differentially modulate Parv+ neurons. Consistent with that, both Parv+ soma and dendrites received more VGlut1+ than VGlut2+ terminals. However, the proportion of VGlut1+ terminal targeting onto Parv+ proximal and distal dendrites was not different, but VGlut2+ terminals tended to target Parv+ somas and proximal dendrites than distal dendrites. These functional and morphological results suggested excitatory cortical and thalamic glutamatergic inputs differently modulate Parv+ interneurons, which provided inhibition inputs onto striatal projection neurons. To maintain the balance between the cortex and thalamus onto Parv+ interneurons may be an important therapeutic target for neurological disorders.

Keywords Parvalbumin interneuron · Glutamatergic synapses · Striatum · Cortex · Thalamus

Xuefeng Zheng, Liping Sun and Bingbing Liu have contributed equally to this article.

✉ Wanlong Lei
leiw@mail.sysu.edu.cn

- ¹ Department of Anatomy, Zhongshan School of Medicine, Sun Yat-Sen University, Guangzhou, China
- ² Department of Anatomy, Neuroscience Laboratory for Cognitive and Developmental Disorders, Medical College of Jinan University, Guangzhou, China
- ³ Department of Pathology, School of Basic Medical Sciences, Southern Medical University, Guangzhou, China
- ⁴ Department of Anesthesiology, Guangdong Second Provincial General Hospital, Guangzhou, China
- ⁵ Institute of Medicine, College of Medicine, Jishou University, Jishou, China
- ⁶ The Second School of Clinical Medicine, Southern Medical University, Guangzhou, China

Introduction

The striatum is the major input nucleus of the basal ganglia, which is involved in the control and execution of goal-directed behaviors and habits [1, 2]. Spiny projection neurons (SPNs) are the principal neurons of the striatum and constitute 90–95% of all striatal neurons in rodents, and interneurons only account for 5–10% of all striatal neurons [3]. SPNs can be divided into two populations based on their selective expression of dopamine (DA) receptor subtypes. Direct pathway SPNs (dSPNs) directly project to the internal segment of the globus pallidus (GPi) and the substantia nigra pars reticulata (SNr) and express D1 receptors (D1Rs) and substance P (SP). In contrast, indirect pathway SPNs (iSPNs) mainly project to the external segment of the globus pallidus (GPe) and express D2 receptors (D2Rs) and enkephalin (ENK) [4–6]. Striatal interneurons consist of four types of neurons: cholinergic interneurons

(ChIs) and three populations of GABAergic interneurons comprising parvalbumin (Parv)-expressing fast-spiking interneurons (FSIs), calretinin (CR)-expressing interneurons and neuropeptide Y (NPY)/somatostatin/nitric oxide synthase (NOS)-expressing low-threshold spike interneurons [7–9]. Interneurons are essential for striatal outputs, exerting a powerful feed-forward inhibitory effect on SPNs [10, 11]. Parv+ interneurons represent fewer than 2% of all striatal neurons, but they are the main source of inhibitory GABAergic control of SPNs, which have widely divergent outputs and mutual electrotonic couplings [12, 13]. Parv+ interneurons also play a key role in numerous brain diseases, such as epilepsy, schizophrenia, depression, autism, Alzheimer's disease, and Parkinson's disease [3, 14, 15]. Synaptic organization determines physiological functions. Electrophysiological studies have shown that Parv+ neurons target SPNs and form strong synapses on the proximal somatodendritic region [10].

The striatum receives excitatory glutamatergic inputs mainly from the cerebral cortex and thalamus, and these afferents form asymmetric synapses with postsynaptic structures in the striatum [16–22]. It is generally accepted that vesicular glutamate transporter 1 (VGLut1) and vesicular glutamate transporter 2 (VGLut2) are specific markers that can distinguish between cortical afferents and thalamic afferents in the striatum [23, 24]. Cortical neurons that innervate the striatum express VGLut1, whereas, thalamic afferents are mainly from the parafascicular nucleus (PFn) of the thalamus, and express VGLut2 [23, 24]. Cortical and thalamic projections show distinct distributions in the striatum. Studies have shown that afferents from the cortex and from PFn converge upon the same part of the striatum; thus, striatal interneurons and SPNs probably share common excitatory glutamatergic inputs [9]. However, cortical and thalamic terminals are differentially distributed on different neurons. Afferents from the cortex form synapses on the spines of SPNs, whereas terminals originating from the PFn form synaptic contractions with dendritic shafts [17, 25]. Morphological studies have indicated that cholinergic interneurons in the striatum receive only sparse inputs from cortical fibers and robust glutamatergic inputs of thalamic origin [26–29]. In contrast, NPY interneurons receive inputs from the cortex but not from the thalamus [30, 31]. Previous studies have also confirmed that cortical and thalamic terminals tend to be distributed on specific subcellular structures. Both the dSPN and iSPN receive numerous glutamatergic afferents, but cortical axon terminals connect mainly to heads of the spines on SPNs, whereas thalamic inputs preferentially synaptically connect with spines and many with dendritic shafts [17, 19, 28, 32]. In addition, different synaptic distribution patterns on neurons have different effects on the formation of functional

assemblies [10, 33]. For instance, at the subcellular level, inhibitory interneurons that target dendrites regulate excitability and plasticity, whereas interneurons that target soma control spiking and synchronize functional assemblies of active principal neurons [33]. Previous evidence confirmed that Parv+ neurons received excitatory inputs from both the cortex and thalamus [34–37]. Optogenetic stimulation showed that cortical and thalamic glutamatergic inputs differentially modulate the firing activity of Parv+ neurons through specific intrinsic and synaptic properties [38]. However, few morphological studies have reported the synaptic connection characteristics of cortical and thalamic terminals on striatal Parv+ neurons.

It is unclear whether Parv+ neurons tend to accept one of the two glutamatergic endings and whether the two kinds of endings are differentially distributed on Parv+ subcellular structures [38–41]. C-Jun belongs to the immune-early gene (IEG) family, which plays a crucial role in cellular events [42]. In vitro and in vivo experiments have suggested that IEGs act as “third messengers” and provide neurons with the ability to translate extracellular stimulation into long-term adaptive cellular responses by activating genetic programs [43]. Previous studies have shown that the protein product of the IEG is synthesized in brain and spinal cord following electrical stimulation and induction of kindling as well as noxious stimulation of peripheral somatosensory cells [44, 45]. Thus, electrical stimulation, immunofluorescence and immunoelectron microscopy (immuno-EM) were used to examine the functional and morphological characteristics of synaptic connections formed by Parv+ neurons and terminals of cortical and thalamic inputs.

Materials and Methods

Animals and Groups

All animal experiments were performed according to the National Institutes of Health Guide for the Care and Use of Laboratory Animals conducted and approved by the Animal Care and Use Committee of Sun Yat-sen University (ethical permission No.: Zhongshan Medical Ethics 2014-23). Twenty four adult male SD (Sprague–Dawley) rats weighing 250–300 g used in this study obtained from Laboratory Animal Center of Sun Yet-Sen University (license no. SYXK (Yue) 2015-0107), and these rats were housed under a 12 h light/dark cycle with access to food and water. Rats were randomly divided into three groups: normal group ($n = 12$; six rats were used for immuno-fluorescence, six rats for immuno-EM detection), M1 stimulation group ($n = 6$), PFn stimulation group ($n = 6$).

Electrical Stimulation

The surgical procedures for the electrical stimulation have been described in previous articles [44, 46–49]. Briefly, rats were anesthetized with sodium pentobarbital (50 mg/kg, i.p.), and then placed on a Kopf stereotaxic instrument (catalog no. 60191, Stoelting Co.). The skull was exposed, and then drilled a hole on the right skull (M1 coordinates: ML: –2.5 mm, AP: 1.2 mm, DV: 2.0 mm; PFn coordinates: ML: –1.2 mm, AP: –4.16 mm, DV: –5.5 mm). A stainless steel electrode was inserted into the M1 or PFn of rats in the corresponding group. Biphasic 100 Hz, 0.5 ms current pulses were delivered for 15 min by a electrical stimulators (Master-8, AMPI) [50]. The intensity of the stimulation was adjusted to produce contralateral limb movement. Under anesthetized condition, all rats were transcardially perfused 1 h after stimulation for immunofluorescence.

Immunofluorescence and Immuno-EM

After anesthetized with sodium pentobarbital (50 mg/kg, i.p.), rats for immunofluorescence were transcardially perfused with 0.9% saline (400 ml), followed by 400 ml of 4% paraformaldehyde-15% saturated picric acid in 0.1 M PB (phosphate buffer, PB; pH 7.4). Rats for immuno-EM were performed in the same way, but 0.6% glutaraldehyde added in the fixative. All brains were quickly removed and immersed in 4% paraformaldehyde-15% saturated picric acid in 0.1 M PB overnight at 4 °C, then sectioned at 50 µm by vibratome (catalog no. VT1200S, Leica). Sections were pre-treated with 1% sodium borohydride in 0.1 M PB for 30 min followed by 0.3% H₂O₂ in 0.1 M PB (pH 7.4) for 30 min, then incubated for 48 h at 4 °C in 0.1 M PB containing 1% bovine serum albumin without (as negative control samples) or with primary antibody: guinea pig anti-VGlu1 (1:1000, catalog no. AB5905, Millipore), guinea pig anti-VGlu2 (1:2000, catalog no. AB2251-I, Millipore), rabbit anti-c-Jun (1:500, catalog no. 06-225, Millipore) and mouse anti-Parv (1:1000, catalog no. P3088, Sigma-Aldrich).

Sections for immunofluorescence were subsequently rinsed and incubated with secondary antibodies for 1 h at room temperature: alexa fluor 594 conjunct donkey-anti-mouse IgG (1:500, catalog no. 715-585-150, Jackson), alexa fluor 488 conjunct donkey-anti-guinea pig IgG (1:500, catalog no. 706-545-148, Jackson) and alexa fluor 647 conjunct donkey-anti-guinea pig IgG (1:500, catalog no. 711-605-152, Jackson). After rinsed in PB for three times, sections were mounted onto gelatin-coated slides, covered with Fluoro-Gel with TES buffer (catalog no. 17985-30, Electron microscopy sciences). Fluorescent images were acquired using a laser scanning confocal microscope (LSCM, catalog no. Eclipse Ni-E, Nikon). Z-stack digital images were

captured for double-labeling immunofluorescence of VGlu and Parv, and Imaris software (Bitplane, Oxford Instruments Company) was used to created three dimensions (3D) reconstruction and measurements.

Sections for immuno-EM were subsequently rinsed and incubated with secondary antibodies for 3 h at room temperature: biotinylated donkey-anti-guinea pig IgG (1:100, catalog no. 706-065-148, Jackson) and biotinylated horse-anti-mouse IgG (1:100, catalog no. BA2001, VECTOR labs). Section were rinsed 5 min in PB for three times, and then incubated with avidin–biotin solution (1:200, catalog no. PK-6100, VECTOR labs) for 1 h at room temperature, sections were then rinsed 5 min in 0.1 M PB for three times. After PB rinses, sections were immersed in 0.05% DAB (catalog no. D5637, Sigma) in 0.1 M PB for 15 min. Then H₂O₂ (Hydrogen proxide, H₂O₂) was added into the solution with a final concentration of 0.01%, and the sections were incubated in this solution for additional 5 min. Sections were subsequently washed in PB for six times. After DAB visualization, sections were rinsed in 0.1 M sodium cacodylate buffer (catalog no. 6131-99-3, Xiya reagent), then postfixed for 1 h in 2% OsO₄ (osmium tetroxide, OsO₄; catalog no. 18456, PELCO) in 0.1 M sodium cacodylate buffer, dehydrated in a graded series of ethyl alcohols, and then impregnated with 1% uranyl acetate in 100% alcohol and flat embedded in EPON 812 resin (catalog no. 18010, PELCO). Ultrathin sections were cut with an ultramicrotome (catalog no. EM UC6, Leica). The sections were mounted on mesh grids, stained with 0.4% lead citrate and 4.0% uranyl acetate, and finally viewed and photographed with a transmission electron microscope (TEM; catalog no. Tecnai G2 Spirit Twin, FEI company).

Data Collection and Statistical Analysis

According to the atlas of Paxinos and Watson [51], the sections were taken from the interaural plane levels approximately (from 10.70 to 8.74 mm). We focus on the dorso-lateral striatum region, which is closely related to motor functions [3, 52]. For each striatal level, adjacent sections were immunolabeled, light microscope (LM) observation showed that VGlu1+ and VGlu2+ terminals, Parv+ and c-Jun+ neurons were uniformly distributed throughout the striatum. The investigators were blinded to measure different experimental groups.

Counting methods for the density of neurons and terminals were performed as previously described [53–56]. Briefly, densities of Parv+ or c-Jun+ neurons were counted in five randomly selected squares with side lengths as 200 µm. Methods for investigating the connection between VGlu terminals and Parv+ neurons were described in

a published article [56]. Briefly, five 100 μm^2 areas on Parv+ somas were randomly selected in Imaris software, and the number of VGult terminals in this area was used as the density of VGlut terminals on Parv+ somas. To measure the density of corticostriatal and thalamostriatal terminals on Parv+ dendrites, we traced 20 Parv+ dendrites from their soma origins to their endings, and divided it equally into two segments. We took the number of VGlut terminals per 50 μm on the proximal half and the distal half as terminal densities.

For immuno-EM, the data were based on 40 EM images per animal. To only use tissue with adequate antibody penetration, EM analyses were restricted to ultrathin sections from the most superficial sections of blocks. The size of the terminals was determined by measuring them at their widest diameter parallel to and 0.1 μm before the presynaptic membrane. VGlut terminals and Parv+ structures were recognized by immunoreactivity products. Spines were identifiable by their small size, continuity with dendrites, prominent PSD and/or the presence of the spine apparatus. Dendrites were identifiable by their size, oval or elongated shape, and the presence of microtubules and mitochondria [25, 57, 58].

SPSS 20.0 software was used for statistical analyses. The experimental data of each animal was counted as a separate data, and all statistical results were expressed as the mean \pm SD (standard deviation, SD). Comparisons between two groups were examined using Student's *t* test. In all cases, $P < 0.05$ was considered statistically significant.

Results

The Ultrastructural Characteristics of Striatal Parv+ Neurons

The Ultrastructure of Parv+ somas and Dendrites

Immunohistochemistry is an effective technique to specifically label striatal Parv neurons [53, 59]. The present immuno-EM observation showed that Parv positive products were mainly located in neuronal somas, dendrites and axons in the dorsolateral striatum (Fig. 1). Further exploration showed that Parv+ somas were oval or round in shape with a mean size of $13.26 \pm 2.33 \mu\text{m}$, and their cytoplasm was rich in various organelles, such as endoplasmic reticula, Golgi apparatus and mitochondria (Fig. 1a, a'). Moreover, Parv+ dendrites were abundant and smooth with few spines (Fig. 1b, b'). Experimental exploration showed that Parv+ somas and dendrites mainly received asymmetric synaptic inputs, in which each Parv+ soma received 2.47 ± 1.24 (based on 53 Parv+ somas from six rats) asymmetric synaptic inputs, with a mean terminal size

of $0.89 \pm 0.27 \mu\text{m}$ (based on 130 terminals from six rats, Fig. 2a, b). Each Parv+ dendrite received less (1.52 ± 0.66 , based on 220 Parv+ dendrites from six rats) synaptic input than Parv+ somas ($P < 0.05$, Fig. 2a), and the size of terminals on Parv+ dendrites ($0.71 \pm 0.19 \mu\text{m}$, based on 156 terminals from six rats) was slightly smaller than that on Parv+ somas ($0.89 \pm 0.27 \mu\text{m}$, $P < 0.05$, Fig. 2b).

The Morphological Feature for Parv+ Terminals

Immuno-EM results showed that striatal Parv+ terminals were mostly oval or round in shape, and contained a large number of evenly distributed, small spherical vesicles. The EM results showed that the Parv+ terminal size ranged from 0.37 to 1.52 μm , with a mean size of $0.91 \pm 0.31 \mu\text{m}$. Statistical analysis of the size-frequency distributions showed that 76.92% of Parv+ terminals fell into the 0.7–1.5 μm range (based on 102 terminals from six rats, Fig. 2c) [60, 61]. Parv+ terminals made typical symmetrical synaptic contacts with Parv– somas (Fig. 1c) dendrites (Fig. 1c'), and spine bases (Fig. 1d, d'). Our experiment hardly observed any Parv+ terminals targeting onto spine heads. The statistical data showed that $35.86 \pm 5.2\%$ of Parv+ terminals made axo-somatic synapse connections, $52.24 \pm 5.09\%$ made axo-dendritic synapses, and $8.90 \pm 1.49\%$ made axo-spinous synapses (based on 102 terminals from six rats, Fig. 2d). Of most interest was that the spine base targeted by the Parv+ terminal simultaneously received an excitatory input at its head (Fig. 1d, d'). The size of Parv+ terminals targeting the soma was $0.98 \pm 0.37 \mu\text{m}$, $0.88 \pm 0.26 \mu\text{m}$ for axo-dendritic, and $0.66 \pm 0.18 \mu\text{m}$ for axo-spinous synapses, among which there were no significant differences (based on 102 terminals from six rats, $P > 0.05$, Fig. 2e).

Synaptic Characteristics of Striatal Parv Neurons with Cortical and Thalamic Glutamatergic Inputs

Responses of Striatal Parv Neurons to Electrical Stimulation of Cortex M1 and Thalamus PFn

C-Jun is an immediate early gene associated with neuronal excitation in the central nervous system [44, 46–49]. The present experiment utilized electrical stimulation of M1 and PFn and then measured c-Jun expression levels by immunofluorescence labeling to indirectly certify the synaptic connection between striatal Parv neurons and cortical or thalamic afferents. Double-label immunofluorescence results showed that Parv+ and c-Jun+ neurons were distributed uniformly across the dorsolateral striatum, and the percentage of c-Jun/Parv double-labeled neurons made up $20.08 \pm 1.94\%$ of Parv neurons in the M1 stimulation group, and $13.56 \pm 1.26\%$ of the PFn stimulation group, and there

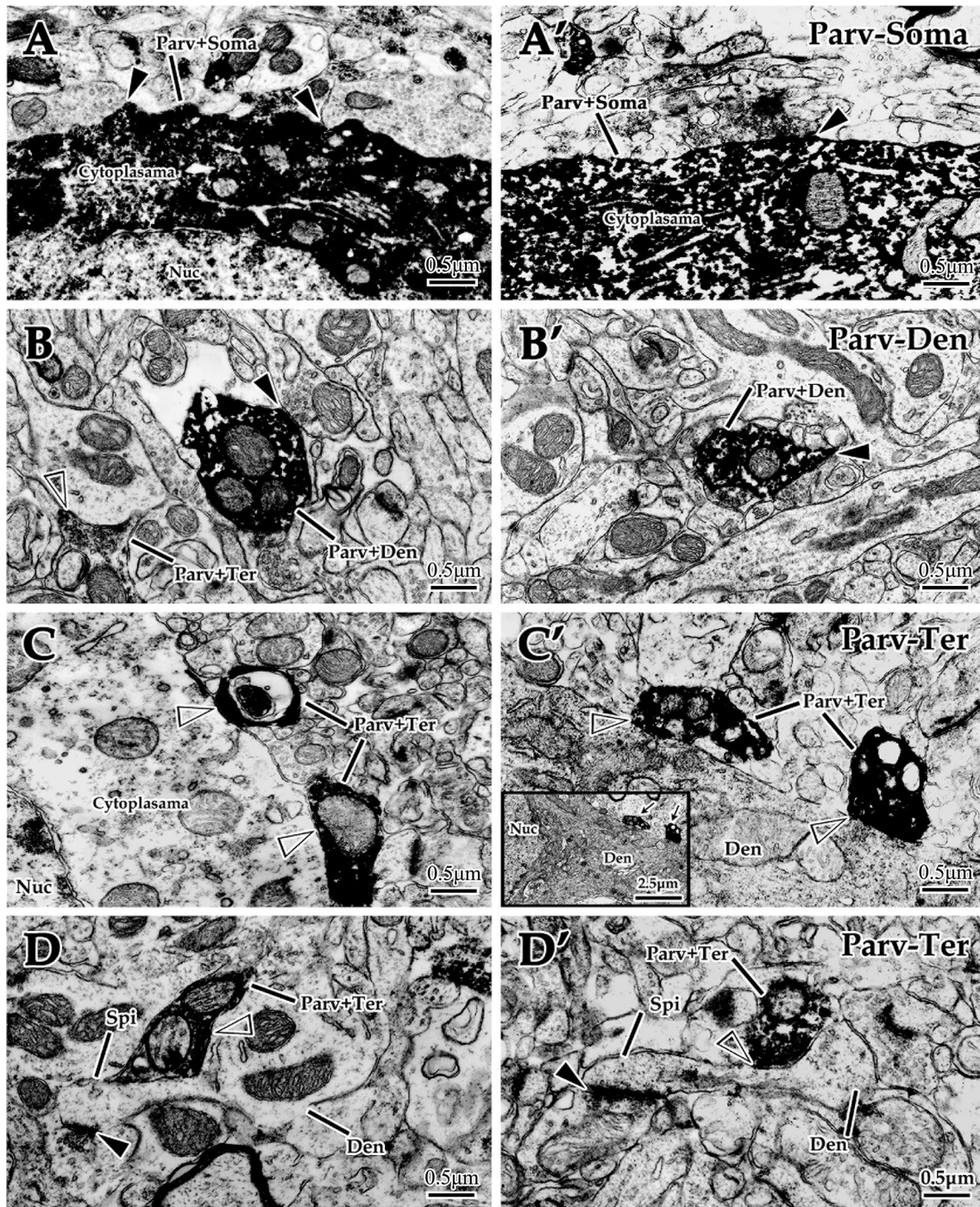
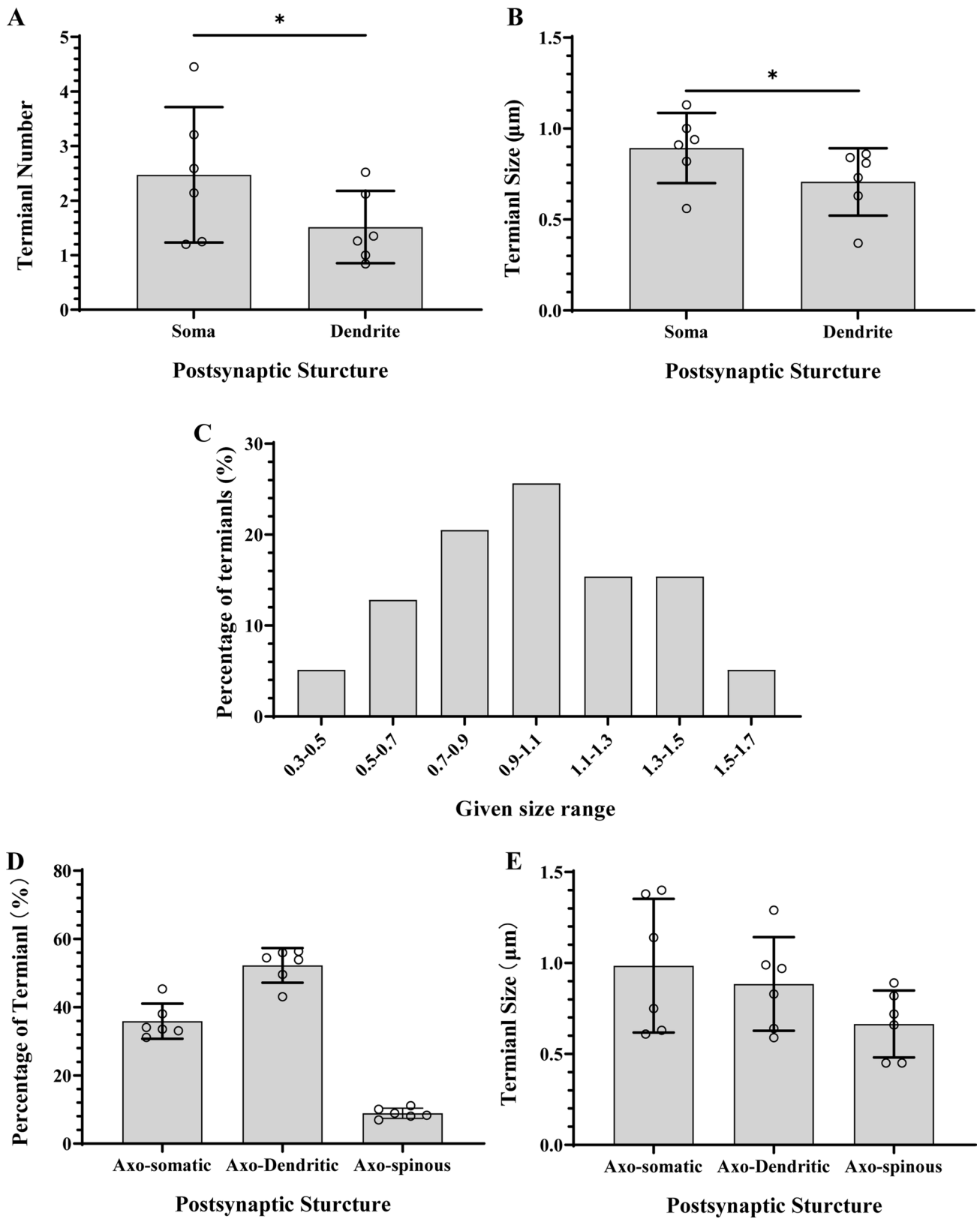


Fig. 1 Morphological characteristics of Parv+neurons. The images show that Parv+somas (**a** and **a'** are two images of axo-somatic synapses) and dendrites (**b** and **b'** are two images of axo-dendritic synapses) received asymmetric synaptic inputs (**▲**), and Parv+ terminals made symmetric synaptic connections (**△**) with Parv− somas (**c**), root of dendrites (**c'**) and the bases of spines (**d** and **d'** are two images

of axo-spinous synapses) whose heads received asymmetric synaptic input (**▲**). *White arrowheads* (**△**) indicate symmetric synapses. *Black arrowheads* (**▲**) indicate asymmetric synapses. *Parv+* parvalbumin immunoreaction; *Nuc* nucleus; *Den* dendrite; *Ter* terminal; *Spi* spine. All panels are the same magnification; scale bar=0.5 μm



◀**Fig. 2** The statistical results of synaptic connections formed by Parv+interneurons. Histogram **a** shows the number of terminals targeting Parv+soma (based on 53 Parv+somas from six rats) and dendrite (based on 220 Parv+dendrites from six rats). Histogram **b** shows the size of terminals targeting Parv+soma (based on 130 terminals from six rats) and dendrite (based on 156 terminals from six rats). Histogram **c** shows size-frequency distribution of Parv+synaptic terminals (based on 102 terminals in six rats). Histogram **d** shows the percentage of axo-somatic, axo-dendritic and axo-spinous synapses formed by Parv+terminals (based on 102 terminals in six rats). Histogram **e** shows the size of Parv+terminals that formed axo-somatic, axo-dendritic and axo-spinous synapses (based on 102 terminals in six rats). * indicates $P < 0.05$

was a significant difference between them (Fig. 3, $P < 0.05$). This evidence indicated that cortical- and thalamic- inputs differentially modulate Parv+ neurons.

Immunofluorescence Double-Labeling Detection of Striatal Parv Neurons with Cortical or Thalamic Glutamatergic Terminals

Immunofluorescence double-labeling was utilized to verify the connection for Parv neurons with glutamatergic inputs in the present experiment. The results showed that the VGlut1+ (Fig. 4a) and VGlut2+ (Fig. 4a') terminals were uniformly distributed in the striatum, and formed clear close appositions with Parv+ cell bodies and dendrites. Enumeration data showed that $6.09 \pm 1.17\%$ of all VGlut1+ terminals formed a close apposition with Parv+ neurons, $9.77 \pm 0.50\%$ of them targeted Parv+ soma, $45.79 \pm 3.03\%$ onto Parv+ proximal dendrites and $44.44 \pm 3.37\%$ onto Parv+ distal dendrites (Fig. 4a–e). Comparison results showed that more VGlut1 terminals targeted Parv+ dendrites ($90.23 \pm 6.40\%$) than Parv+ somas ($9.77 \pm 0.50\%$, $P < 0.05$), but there was no difference between the proportion of VGlut1 terminals on proximal dendrites ($45.79 \pm 3.03\%$) and distal segments ($44.44 \pm 3.37\%$, $P > 0.05$, Fig. 4b–e). On the other hand, $6.03 \pm 0.70\%$ of the total VGlut2+ terminals formed a close apposition with Parv+ neurons, of which $8.85 \pm 0.42\%$ targeted Parv+ soma, and $52.62 \pm 11.28\%$ targeted proximal dendrites, which was significantly higher than the percentage targeting distal segments ($38.53 \pm 4.70\%$, $P < 0.05$, Fig. 4a'–d', e). Additionally, the comparative results showed that a higher proportion of VGlut2 terminals targeted Parv+ soma ($9.77 \pm 0.50\%$ for VGlut1, $8.85 \pm 0.42\%$ for VGlut2, $P < 0.05$, Fig. 4b, b', e) and Parv+ proximal dendrites ($45.79 \pm 3.03\%$ for VGlut1, $52.62 \pm 11.28\%$ for VGlut2, $P < 0.05$, Fig. 4c, c', e) than VGlut1, whereas the proportion of VGlut1+ terminals ($44.44 \pm 3.37\%$) connected with Parv+ distal dendrites was higher than that connected on VGlut2+ ($38.53 \pm 4.70\%$, $P < 0.05$, Fig. 4d, d', e).

Ultrastructural Characteristics of VGlut1+ and VGlut2+ Terminals Targeting Parv Neurons

The present experiment by means of immuno-EM double-labeling for VGluts with Parv aimed to investigate the ultrastructure characteristics of cortical or thalamic terminals targeting Parv neurons. Experimental results showed that VGlut1+ and VGlut2+ terminals were uniformly distributed throughout the dorsolateral striatum. Our previous studies revealed the ultrastructural characteristics and sizes of VGlut1+ and VGlut2+ terminals in the striatum of rats [58, 61]. In brief, immunoreactivity products were mainly located on synaptic vesicles and gathered adjacent to the presynaptic membrane, and both VGlut1+ and VGlut2+ terminals were round or oval in shape and made asymmetric synaptic connections with different postsynaptic elements. The present exploration showed that VGlut1+ (based on 528 VGlut1+ terminals of six rats) and VGlut2+ terminals (based on 493 VGlut2+ terminals of six rats) targeted either Parv+ or Parv− elements (Fig. 5).

The enumeration data showed that $0.46 \pm 0.08\%$ of VGlut1+ terminals targeted Parv+ somas, and $5.83 \pm 1.09\%$ onto Parv+ dendrites, and there was a significant difference between them ($P < 0.05$, Fig. 5a–d, 6a). Measurement data showed that VGlut1+ terminals targeting Parv+ somas ($0.87 \pm 0.29 \mu\text{m}$) were larger than those targeting Parv+ dendrites (0.71 ± 0.27 , $P < 0.05$, Fig. 5a–d, 6b). Moreover, $5.31 \pm 0.58\%$ of VGlut2+ terminals made asymmetric synaptic connections with Parv+ dendrites, which was higher than that with Parv+ somas ($0.72 \pm 0.12\%$, $P < 0.05$, Fig. 5a'–d', 6a). Measurement data showed that the size of VGlut2+ terminals targeting Parv+ somas was $0.88 \pm 0.26 \mu\text{m}$ and that targeting Parv+ dendrites was $0.55 \pm 0.24 \mu\text{m}$, and there was a significant difference between them ($P < 0.05$, Fig. 5a'–d', 6b). Comparative data between VGlut1+ and VGlut2+ terminals showed that the percentage of VGlut1+ terminals ($0.46 \pm 0.08\%$) targeting Parv+ somas was lower than that of VGlut2+ terminals ($0.72 \pm 0.12\%$, $P < 0.05$, Fig. 6a), and the percentage of VGlut1+ terminals ($5.83 \pm 1.09\%$) targeting Parv+ dendrites was not different from that of VGlut2+ terminals ($5.31 \pm 0.58\%$, $P > 0.05$, Fig. 6a).

Ultrastructural Exploration of Parv Neurons Receiving VGlut1+ or VGlut2+ Synaptic Inputs

As above immuno-EM single-labeling results on Parv+ neurons (Fig. 1), the present immuno-EM double-labeling experiment for Parv+ neurons with VGluts+ terminals (Fig. 5) showed that Parv+ somas and dendrites, and VGlut1+ or VGlut2+ terminals, as well as their synapse connection were distinctly observed in the

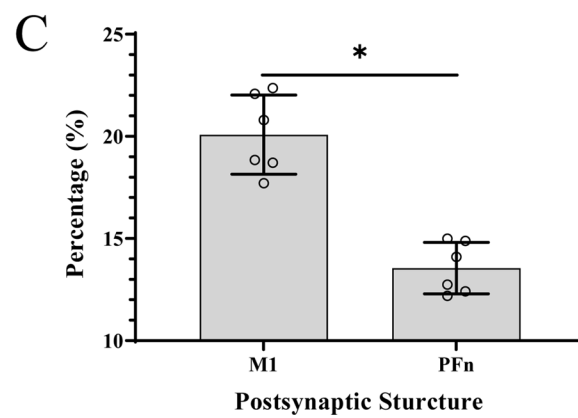
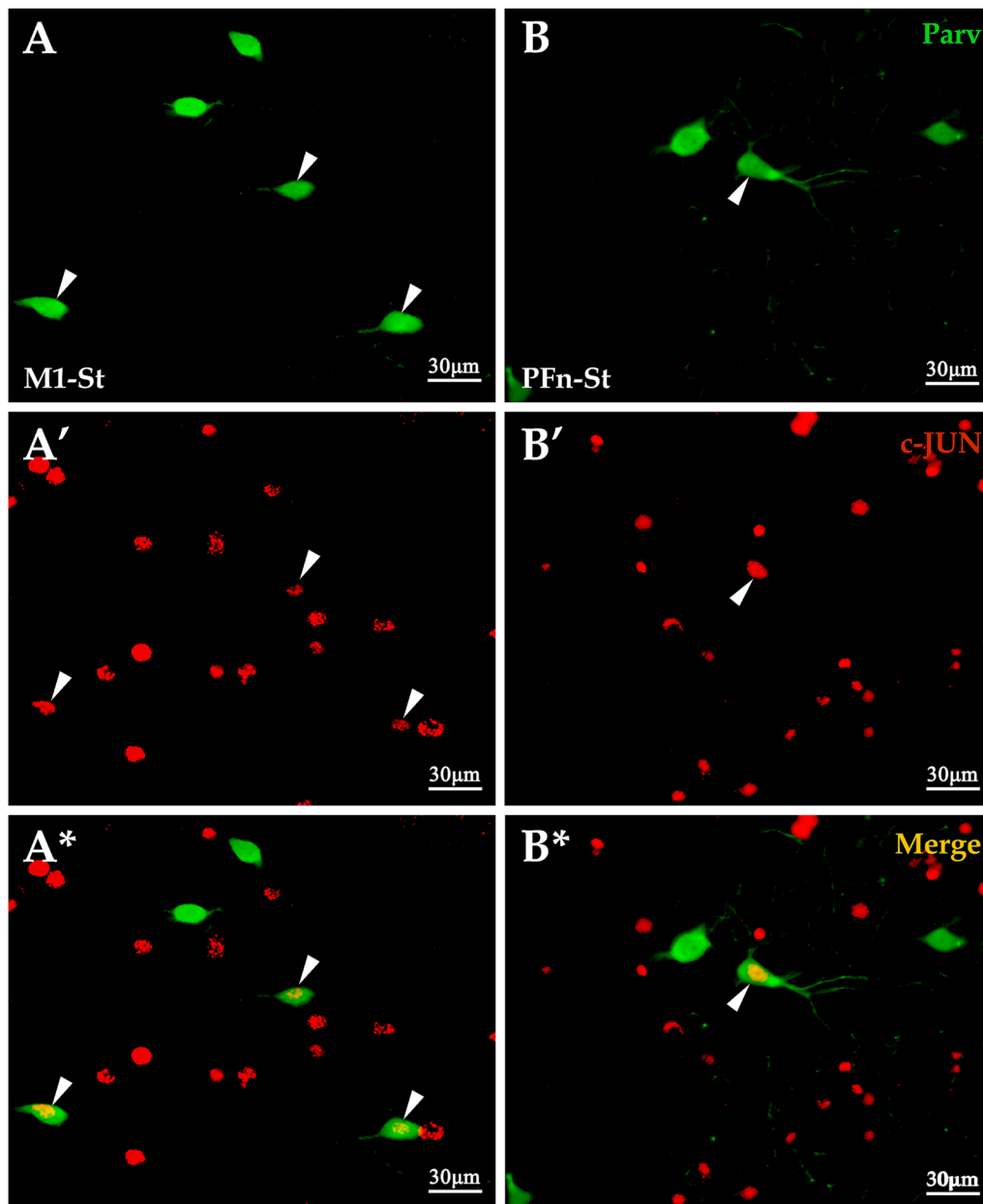


Fig. 3 Responses of Parv+ neurons to M1 and PFn stimulation. To functionally assess the difference between cortical- and thalamic-inputs on striatal neurons, electrical stimulation was performed in M1 (**a**, **a'**, **a***) and PFn (**b**, **b'**, **b***). Images **a** and **b** show Parv+ cells in the striatum. Images **a'** and **b'** show c-Jun+ cells in the striatum. Images **a*** and **b*** are merged images of **a** and **b**, **a'** and **b'**, respectively. White arrowheads (Δ) indicate the colocalization of Parv+ and c-Jun+ neurons. All images show the same magnification; scale bar = 30 μ m. Histogram **c** shows the percentage of c-Jun/Parv double-labeled neurons in the M1 stimulation group and the PFn stimulation group. * indicates $P < 0.05$

dorsolateral striatum. Immuno-EM showed that striatal Parv+ somas and dendrites received either VGLuts positive synaptic inputs or VGLuts negative synaptic inputs (Fig. 5). Statistical data showed that $80.20 \pm 10.65\%$ of Parv+ somas (based on 62 Parv+ somas of six rats) received VGLut1+ synaptic inputs, $70.55 \pm 12.28\%$ of Parv+ dendrites (based on 225 Parv+ dendrites of six rats) received VGLut1+ synaptic inputs, and there was no significant difference between them ($P > 0.05$, Fig. 6c). The VGLut1+ terminal size was described above (Fig. 6b). Similarly, $57.70 \pm 12.56\%$ of Parv+ somas (based on 58 Parv+ somas of six rats) received VGLut2+ synaptic inputs, $48.34 \pm 9.52\%$ of Parv+ dendrites (based on 193 Parv+ dendrites of six rats) received VGLut2+ synaptic inputs, and there was no difference between them ($P > 0.05$, Fig. 6c). The VGLut2+ terminal size was described above (Fig. 6b). Thus, Parv+ neurons were targeted by both VGLut1+ and VGLut2+ terminals, but in fact further comparative results indicated that Parv+ neurons were preferably targeted by VGLut1+ terminals. The proportion of somas and dendrites receiving VGLut1+ inputs was significantly higher than that receiving VGLut2 ($P < 0.05$, Fig. 6c). In addition, Parv+ dendrites connected with VGLut2+ terminals (1.75 ± 0.76) were thicker than those connected with VGLut1+ terminals (1.13 ± 0.47 , $P < 0.05$, Fig. 5b–d', Fig. 6d), which means that VGLut2 terminals tended to target proximal dendrites.

Comparative results showed that Parv+ somas received more VGLut1+ synaptic (1.18 ± 0.15) than VGLut2+ inputs (0.80 ± 0.14 , $P < 0.05$, Fig. 6e), and Parv+ dendrites also received more VGLut1+ terminals (0.73 ± 0.12) than VGLut2+ terminals (0.50 ± 0.15 , $P < 0.05$, Fig. 6e). Additionally, no significant difference was observed between the VGLut1+ (0.87 ± 0.29) and VGLut2+ (0.88 ± 0.26) terminal sizes on Parv+ somas ($P > 0.05$, Fig. 6b), whereas Parv+ dendrites received larger VGLut1+ terminals (0.71 ± 0.27) than VGLut2+ terminals (0.55 ± 0.24 , $P < 0.05$, Fig. 6b).

Discussion

The main findings of the present study show that (1) both Parv+ somas and dendrites receive numerous asymmetric synaptic inputs, and Parv+ terminals form asymmetric synapses with Parv– somas, dendrites and spine bases. Most interestingly, spine bases targeted by Parv+ terminals simultaneously received excitatory inputs at their heads. (2) Electrical stimulation of the motor cortex (M1) induced more Parv+ neurons to express c-Jun than stimulation of the parafascicular nucleus (PFN) of the thalamus, indicating that cortical- and thalamic-inputs differentially modulate Parv+ neurons. (3) Immunofluorescence and immunoelectro microscopy experiments showed that the majority of VGLut+ terminals targeted Parv– elements, and a few targeted Parv+ elements. On the other hand, both Parv+ somas and dendrites received more VGLut1+ terminals than VGLut2+ terminals. VGLut1+ terminals were uniformly distributed on Parv+ dendrites, but VGLut2+ terminals tended to target Parv+ somas and proximal dendrites rather than distal dendrites.

Parv+ Neurons Produce Feed-Forward Inhibition of SPNs in Response to Thalamic and Cortical Inputs

SPNs are the main output neurons of the striatum and account for the majority of striatal neurons. SPNs can be divided to two populations of similar size: dSPNs that primarily project directly to the internal segment of the globus pallidus and substantia nigra pars reticulata, and iSPNs that project only to the external segment of the globus pallidus and thus are indirectly connected to the output nuclei. The two pathways are differentially modulated by DA, due to their selective expression of DA receptor subtypes. In addition, four subtypes of striatal interneurons were identified, and interneurons are contribute to feed-forward inhibition to regulate the activity of SPNs and are vital for normal striatal functions [3, 39–41]. Parv+ interneurons are the main source of inhibitory GABAergic control of SPNs with widely divergent outputs and mutual electrotonic coupling. Electrophysiological studies have revealed that Parv+ neurons form strong synapses with the proximal dendritic regions of nearby SPNs [10]. In addition, a study showed that Parv+ neurons were the main inhibitory source of SPNs [62, 63]. Here, we provide ultrastructural evidence that terminals of Parv+ neurons form asymmetrical synapses on the somas and dendrites of striatal SPNs. The striatum receives dense glutamatergic inputs from the neocortex and

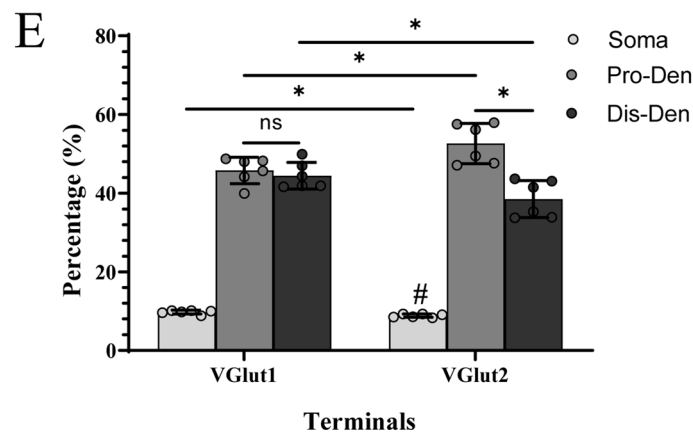
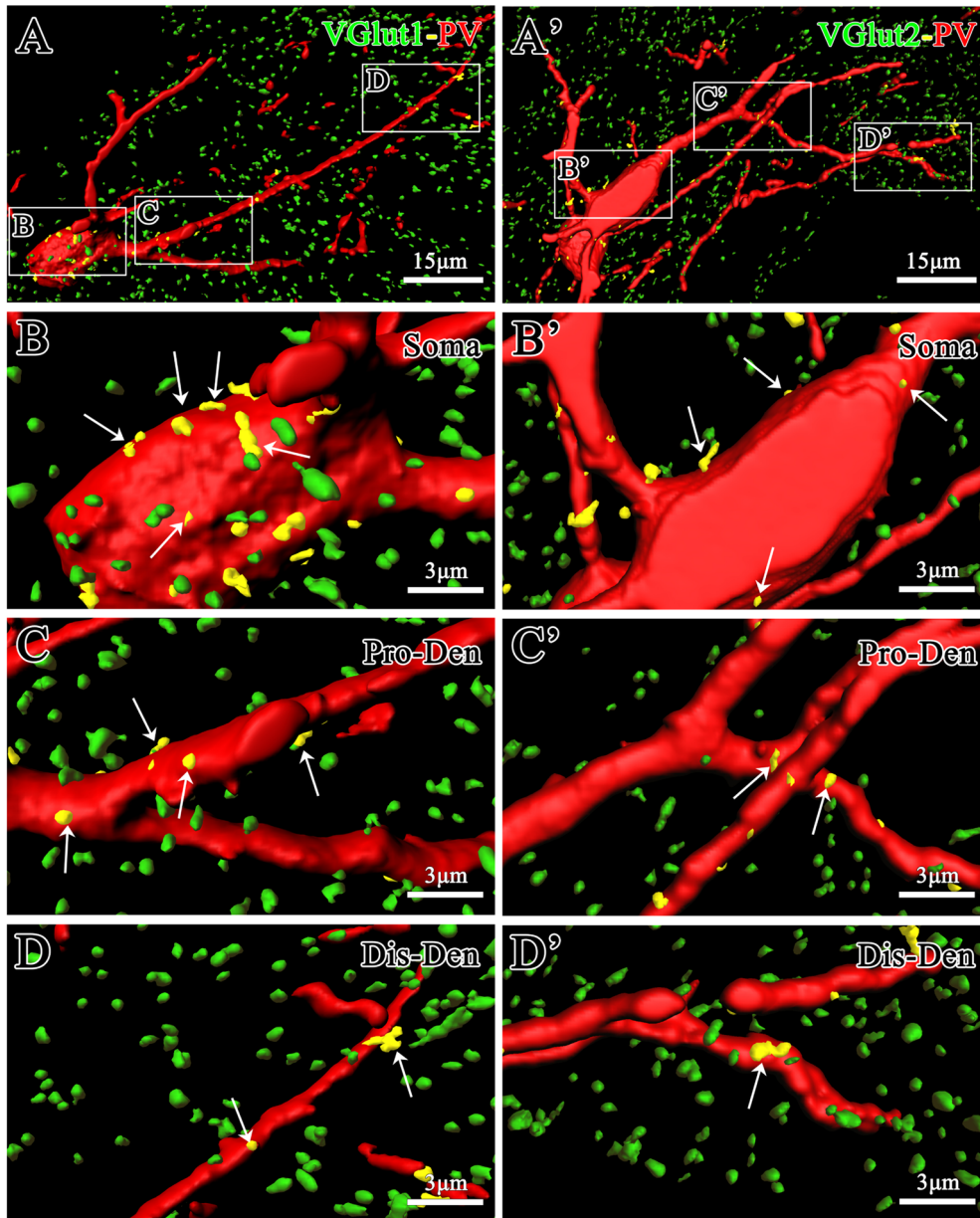


Fig. 4 The close apposition of Parv+ neurons and VGlut+ terminals. Images showing VGlut1 (a–d) and VGlut2 (a'–d') terminals formed close appositions (yellow) on Parv+ interneurons, as demonstrated by 3D reconstructions of double immunofluorescence results with Parv (red) and VGluts (green and yellow) antibodies. Arrows (→) indicate VGluts (yellow) terminals attached to Parv+ (red) somas (b, b'), proximal dendrites (c, c') and distal dendrites (d, d'). Panels b–d and b'–d' are higher magnifications of the corresponding boxed areas in panels a and a', respectively. Panels a and a' show the same magnification; scale bar = 15 μm. Panels b–d and b'–d' show the same magnification; scale bar = 3 μm. Histogram e shows the LM results for the percentage of VGluts terminals at different positions of Parv+ neurons. *Pro-Den* proximal dendrite; *Dis-Den* distal dendrite. * indicates $P < 0.05$

the thalamus [64]. Our previous studies showed that glutamatergic terminals in the striatum mainly formed synaptic connections with SPNs [25, 61, 64]. Moreover, it has been established that striatal Parv+ interneurons receive inputs from the cerebral cortex and thalamus [37, 41]. SPNs and Parv+ neurons share the same glutamatergic inputs from the cortex [65, 66] and PFn [67], and Parv+ neurons form inhibitory synaptic connections with SPNs; thus, they can convert an excitatory input signal from the cortex and the PFn into an inhibitory output signal within a millisecond [39, 41, 68]. In summary, Parv+ interneurons exert powerful feed-forward modulation on SPNs and play a critical role in timing striatal output [63].

In addition, our results showed that a small portion of Parv+ terminals targeted the base of spines on SPNs. It is well known that most glutamatergic inputs from the cortex and thalamus attach to the heads of the spines [69–71]. According to this synaptic pattern, we speculated that in addition to directly inhibiting SPNs, Parv+ neurons could also modulate the excitatory afferents of SPNs [72, 73]. The synchronized firing of Parv+ neurons is sufficient to alter the balance in firing between the direct and indirect pathway neurons of the striatum [10].

Different Regulatory Effects of Cortical and Thalamic Afferents on Parv+ Neurons

SPNs receive extra-striatal synaptic inputs from diverse brain areas, but the majority of their inputs are glutamatergic and arise from cortical and thalamic regions. Understanding the regulatory effects of the cortex and thalamus on the Parv+ interneuron system is critical to reveal its feed-forward function. Studies have revealed that cortical and thalamic terminals have different distribution patterns

on SPNs. Approximately 90% of VGlut1 terminals end on spines, but only 45% of VGlut2 terminals target spines [58, 74, 75]. Our functional experiment showed that stimulation on M1 induced more Parv+ neurons to express c-Jun than PFn stimulation. This evidence suggests that cortical inputs have different synaptic connection patterns on Parv+ interneurons compared with thalamic afferents. In support of this hypothesis, our results further indicated that Parv+ neurons received more cortical inputs than thalamic inputs [35]. Injecting the anterograde tracer biotinylated dextranamine into the PFn of adult rats revealed that only 4% of all asymmetric synapses on Parv+ dendrites were derived from the parafascicular nucleus [35]. However, Nakano et al. revealed that the density of VGlut2 appositions was almost 10 times higher than that determined by anterograde tracer AAV labeling of axons from the mouse thalamus [56]. Thus, approximately 40% of asymmetric synapses on Parv+ terminals should be derived from the thalamus, which is consistent with our ultrastructural results.

In addition to the quantities of terminals, the distribution patterns of cortical and thalamic afferents on Parv+ neurons display differences. These morphological differences may help to explain the different responses of PV neurons to cortex and thalamus stimulation [38, 39]. There was a higher proportion of thalamic terminals distributed in the proximal region of Parv+ neurons, whereas cortical terminals were uniformly distributed on Parv+ dendrites. Thus, thalamostriatal synapse activation produces a larger electric driving force with less attenuation and induces a higher probability of transmitter release than the activation of corticostriatal synapses [38]. In addition, consistent with our results, studies have compared asymmetric inputs to Parv+ neurons indicating that thalamic inputs appear anatomically minor than the cerebral cortex in rats, mice and monkeys [35, 37, 56].

In summary, we provided more morphological evidence to confirm that both striatal SPNs and Parv+ neurons were innervated by corticostriatal and thalamostriatal glutamatergic fibers. Cortical terminals on Parv+ interneurons were denser than thalamic terminals, and thalamic inputs tended to target soma and proximal dendrites, whereas cortical terminals were uniformly distributed along Parv+ dendrites. Growing evidence strongly suggests that structural and functional deficits of Parv+ interneurons are implicated in epilepsy, schizophrenia, and PD [39]. Maintaining the balance between cortical and thalamic inputs on Parv+ interneurons may be an important therapeutic target for human diseases.

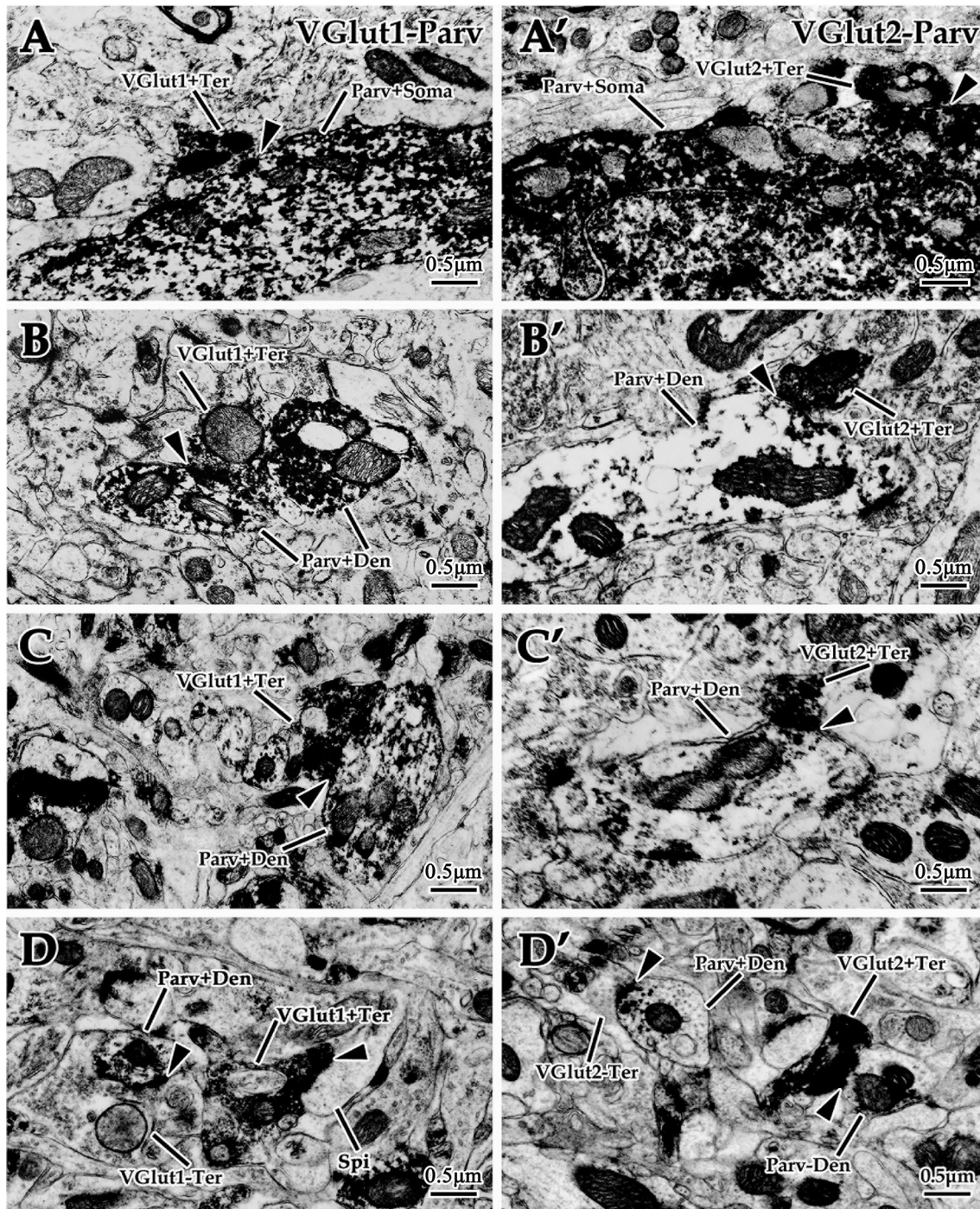


Fig. 5 Ultrastructural characteristics of synapses of Parv+ neurons with VGlut+ terminals. Panels **a–d** show that VGlut1+ terminals formed asymmetric synapses with Parv+ somas (**a**) and dendrites (**b–d**). Panels **a'–d'** showed that VGlut2+ terminals formed asymmetric synapses with Parv+ somas (**a'**) and dendrites (**b'–d'**). In addition,

many VGlut1+ (**d**) and VGlut2+ (**d'**) terminals also targeted Parv– structures. *Black arrowheads* (▲) indicate asymmetric synapses. *Parv+* parvalbumin immune positive reaction; *Parv–* parvalbumin immune negation; *Den* dendrite; *Ter* terminal. All panels are the same magnification; scale bar = 0.5 μm

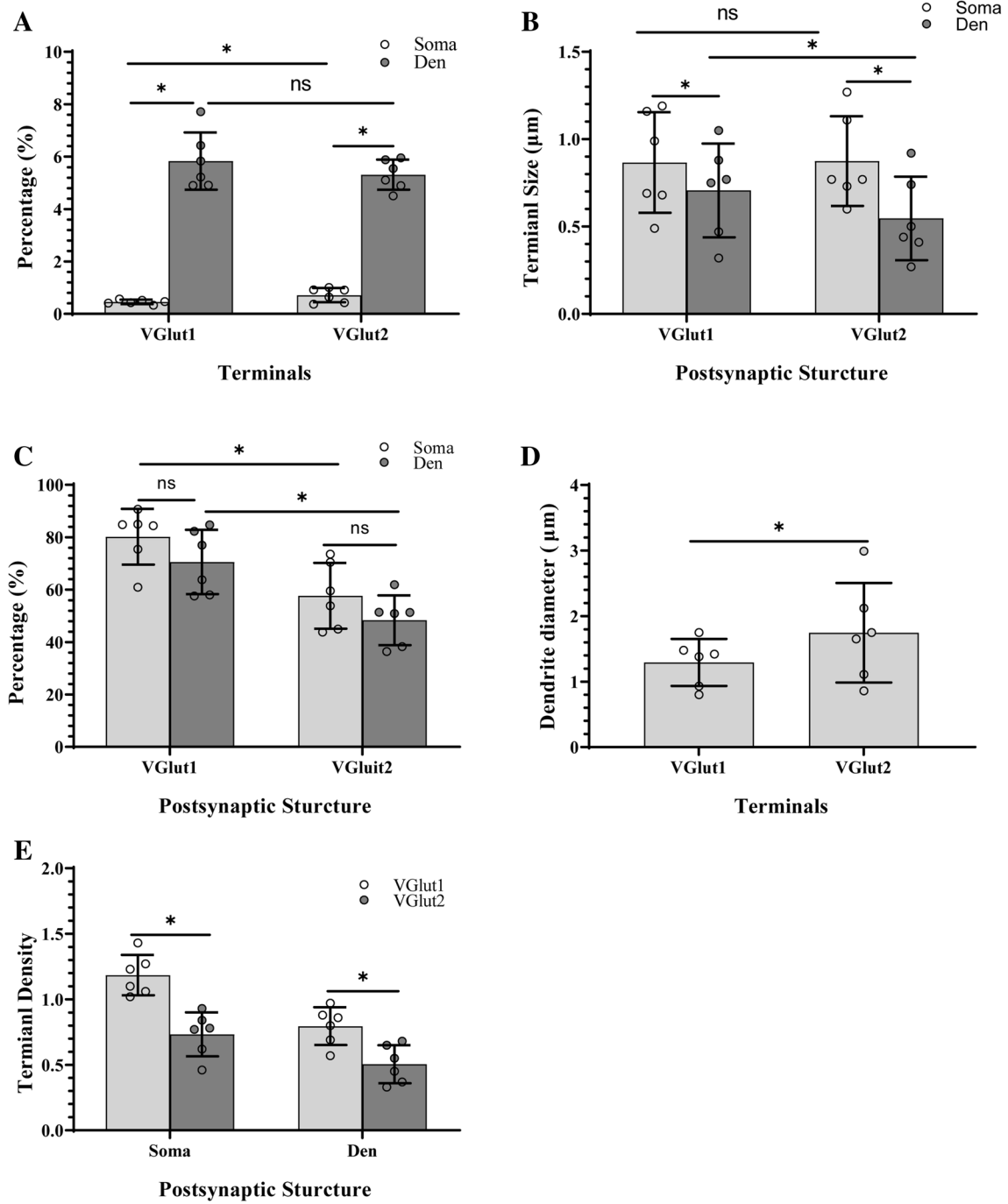


Fig. 6 The statistical results of synaptic connections formed by Vgluts+terminals and Parv+interneurons. Histograms **a** and **b** show the EM results for the percentage **c** and sizes **d** of VGluts terminals on Parv+somas and dendrites. Histogram **c** reveals the percentage of Parv+structures received VGlut1+or VGlut2+inputs. Histo-

gram **d** shows the diameter of Parv+structures received VGlut1+or VGlut2+inputs. Histogram **e** shows the number of VGlut1+or VGlut2+targeting Parv+structures. *Den* dendrite. * indicates $P < 0.05$

Acknowledgements This work was supported by the National Natural Science Foundation of China (81471288), and by the National Key R&D Program of China (2017YFA0104704).

Declarations

Conflict of Interest The authors declare that they have no conflict of interest.

Ethical Approval All animal experiments were performed according to the National Institutes of Health Guide for the Care and Use of Laboratory Animals conducted and approved by the Animal Care and Use Committee of Sun Yat-sen University (ethical permission No.: Zhongshan Medical Ethics 2014-23).

References

- Zhai S, Tanimura A, Graves SM et al (2018) Striatal synapses, circuits, and Parkinson's disease. *Curr Opin Neurobiol* 48:9–16
- Albin RL, Young AB, Penney JB (1989) The functional anatomy of basal ganglia disorders. *Trends Neurosci* 12:366–375
- Gittis AH, Kreitzer AC (2012) Striatal microcircuitry and movement disorders. *Trends Neurosci* 35:557–564
- Gerfen CR, Surmeier DJ (2011) Modulation of striatal projection systems by dopamine. *Annu Rev Neurosci* 34:441–466
- Gerfen CR, Keefe KA, Gauda EB (1995) D1 and D2 dopamine receptor function in the striatum: coactivation of D1- and D2-dopamine receptors on separate populations of neurons results in potentiated immediate early gene response in D1-containing neurons. *J Neurosci* 15:8167–8176
- Gerfen CR, Engber TM, Mahan LC et al (1990) D1 and D2 dopamine receptor-regulated gene expression of striatonigral and striatopallidal neurons. *Science* 250:1429–1432
- Kawaguchi Y (1993) Physiological, morphological, and histochemical characterization of three classes of interneurons in rat neostriatum. *J Neurosci* 13:4908–4923
- Kawaguchi Y, Wilson CJ, Augood SJ et al (1995) Striatal interneurons: chemical, physiological and morphological characterization. *Trends Neurosci* 18:527–535
- Tepper JM, Koos T, Wilson CJ (2004) GABAergic microcircuits in the neostriatum. *Trends Neurosci* 27:662–669
- Straub C, Saulnier JL, Begue A et al (2016) Principles of synaptic organization of GABAergic interneurons in the striatum. *Neuron* 92:84–92
- Silberberg G, Bolam JP (2015) Local and afferent synaptic pathways in the striatal microcircuitry. *Curr Opin Neurobiol* 33:182–187
- Koos T, Tepper JM (1999) Inhibitory control of neostriatal projection neurons by GABAergic interneurons. *Nat Neurosci* 2:467–472
- Cowan RL, Wilson CJ, Emson PC et al (1990) Parvalbumin-containing GABAergic interneurons in the rat neostriatum. *J Comp Neurol* 302:197–205
- Marin O (2012) Interneuron dysfunction in psychiatric disorders. *Nat Rev Neurosci* 13:107–120
- Mallet N, Ballion B, Le Moine C et al (2006) Cortical inputs and GABA interneurons imbalance projection neurons in the striatum of parkinsonian rats. *J Neurosci* 26:3875–3884
- Kitai ST, Kocsis JD, Preston RJ et al (1976) Monosynaptic inputs to caudate neurons identified by intracellular injection of horseradish peroxidase. *Brain Res* 109:601–606
- Dube L, Smith AD, Bolam JP (1988) Identification of synaptic terminals of thalamic or cortical origin in contact with distinct medium-size spiny neurons in the rat neostriatum. *J Comp Neurol* 267:455–471
- Deschenes M, Bourassa J, Doan VD et al (1996) A single-cell study of the axonal projections arising from the posterior intralaminar thalamic nuclei in the rat. *Eur J Neurosci* 8:329–343
- Smith AD, Bolam JP (1990) The neural network of the basal ganglia as revealed by the study of synaptic connections of identified neurones. *Trends Neurosci* 13:259–265
- Berendse HW, Groenewegen HJ (1990) Organization of the thalamostriatal projections in the rat, with special emphasis on the ventral striatum. *J Comp Neurol* 299:187–228
- Gerfen CR (1988) Synaptic organization of the striatum. *J Electron Microscop Tech* 10:265–281
- Herkenham M, Pert CB (1981) Mosaic distribution of opiate receptors, parafascicular projections and acetylcholinesterase in rat striatum. *Nature* 291:415–418
- Lacey CJ, Boyes J, Gerlach O et al (2005) GABA(B) receptors at glutamatergic synapses in the rat striatum. *Neuroscience* 136:1083–1095
- Raju DV, Shah DJ, Wright TM et al (2006) Differential synaptology of vGluT2-containing thalamostriatal afferents between the patch and matrix compartments in rats. *J Comp Neurol* 499:231–243
- Lei W, Jiao Y, Del MN et al (2004) Evidence for differential cortical input to direct pathway versus indirect pathway striatal projection neurons in rats. *J neurosci* 24:8289–8299
- Dimova R, Vuillet J, Nieoullon A et al (1993) Ultrastructural features of the choline acetyltransferase-containing neurons and relationships with nigral dopaminergic and cortical afferent pathways in the rat striatum. *Neuroscience* 53:1059–1071
- Meredith GE, Chang HT (1994) Synaptic relationships of enkephalinergic and cholinergic neurons in the nucleus accumbens of the rat. *Brain Res* 667:67–76
- Lapper SR, Bolam JP (1992) Input from the frontal cortex and the parafascicular nucleus to cholinergic interneurons in the dorsal striatum of the rat. *Neuroscience* 51:533–545
- Meredith GE, Wouterlood FG (1990) Hippocampal and midline thalamic fibers and terminals in relation to the choline acetyltransferase-immunoreactive neurons in nucleus accumbens of the rat: a light and electron microscopic study. *J Comp Neurol* 296:204–221
- Kachidian P, Vuillet J, Nieoullon A et al (1996) Striatal neuropeptide Y neurones are not a target for thalamic afferent fibres. *Neuroreport* 7:1665–1669
- Vuillet J, Kerkerian L, Kachidian P et al (1989) Ultrastructural correlates of functional relationships between nigral dopaminergic or cortical afferent fibers and neuropeptide Y-containing neurons in the rat striatum. *Neurosci Lett* 100:99–104
- Clarke DJ, Dunnett SB (1993) Synaptic relationships between cortical and dopaminergic inputs and intrinsic GABAergic systems within intrastriatal striatal grafts. *J Chem Neuroanat* 6:147–158
- Roux L, Buzsaki G (2015) Tasks for inhibitory interneurons in intact brain circuits. *Neuropharmacology* 88:10–23
- Smith Y, Raju D, Nanda B et al (2009) The thalamostriatal systems: anatomical and functional organization in normal and parkinsonian states. *Brain Res Bull* 78:60–68
- Rudkin TM, Sadikot AF (1999) Thalamic input to parvalbumin-immunoreactive GABAergic interneurons: organization in normal striatum and effect of neonatal decortication. *Neuroscience* 88:1165–1175
- Sidibe M, Smith Y (1999) Thalamic inputs to striatal interneurons in monkeys: synaptic organization and co-localization of calcium binding proteins. *Neuroscience* 89:1189–1208

37. Lapper SR, Smith Y, Sadikot AF et al (1992) Cortical input to parvalbumin-immunoreactive neurones in the putamen of the squirrel monkey. *Brain Res* 580:215–224
38. Sciamanna G, Ponterio G, Mandolesi G et al (2015) Optogenetic stimulation reveals distinct modulatory properties of thalamostriatal vs corticostriatal glutamatergic inputs to fast-spiking interneurons. *Sci Rep* 5:16742
39. Hu H, Gan J, Jonas P (2014) Interneurons. Fast-spiking, parvalbumin(+) GABAergic interneurons: from cellular design to microcircuit function. *Science* 345:1255–1263
40. Kita H, Kosaka T, Heizmann CW (1990) Parvalbumin-immunoreactive neurons in the rat neostriatum: a light and electron microscopic study. *Brain Res* 536:1–15
41. Bennett BD, Bolam JP (1994) Synaptic input and output of parvalbumin-immunoreactive neurons in the neostriatum of the rat. *Neuroscience* 62:707–719
42. Schuermann M, Neuberger M, Hunter JB et al (1989) The leucine repeat motif in Fos protein mediates complex formation with Jun/AP-1 and is required for transformation. *Cell* 56:507–516
43. Herschman HR (1989) Extracellular signals, transcriptional responses and cellular specificity. *Trends Biochem Sci (Amsterdam)* 14:455
44. Herdegen T, Leah JD, Manisali A et al (1991) c-JUN-like immunoreactivity in the CNS of the adult rat: basal and transynaptically induced expression of an immediate-early gene. *Neuroscience* 41:643–654
45. Herdegen T, Kovary K, Leah J et al (1991) Specific temporal and spatial distribution of JUN, FOS, and KROX-24 proteins in spinal neurons following noxious transsynaptic stimulation. *J Comp Neurol* 313:178–191
46. Hunt SP, Pini A, Evan G (1987) Induction of c-fos-like protein in spinal cord neurons following sensory stimulation. *Nature* 328:632–634
47. Pearse DD, Bushell G, Leah JD (2001) Jun, Fos and Krox in the thalamus after C-fiber stimulation: coincident-input-dependent expression, expression across somatotopic boundaries, and nucleolar translocation. *Neuroscience* 107:143–159
48. Li S, Ye F, Farber JP et al (2019) Dependence of c-fos expression on amplitude of high-frequency spinal cord stimulation in a rodent model. *Neuromodulation* 22:172–178
49. Hitier M, Sato G, Zhang YF et al (2018) Effects of electrical stimulation of the rat vestibular labyrinth on c-Fos expression in the hippocampus. *Neurosci Lett* 677:60–64
50. Stiles L, Reynolds JN, Napper R et al (2018) Single neuron activity and c-Fos expression in the rat striatum following electrical stimulation of the peripheral vestibular system. *Physiol Rep* 6:e13791
51. Paxinos GWC (1986) *The rat brain in stereotaxic coordinates*. Elsevier Academic Press, San Diego
52. Kreitzer AC (2009) Physiology and pharmacology of striatal neurons. *Annu Rev Neurosci* 32:127–147
53. Mu S, OuYang L, Liu B et al (2011) Protective effect of melatonin on 3-NP induced striatal interneuron injury in rats. *Neurochem Int* 59:224–234
54. Ma Y, Zhan M, OuYang L et al (2014) The effects of unilateral 6-OHDA lesion in medial forebrain bundle on the motor, cognitive dysfunctions and vulnerability of different striatal interneuron types in rats. *Behav Brain Res* 266:37–45
55. Mu S, Lin E, Liu B et al (2014) Melatonin reduces projection neuronal injury induced by 3-nitropropionic acid in the rat striatum. *Neurodegener Dis* 14:139–150
56. Nakano Y, Karube F, Hirai Y et al (2018) Parvalbumin-producing striatal interneurons receive excitatory inputs onto proximal dendrites from the motor thalamus in male mice. *J Neurosci Res* 96:1186–1207
57. Deng YP, Wong T, Bricker-Anthony C et al (2013) Loss of corticostriatal and thalamostriatal synaptic terminals precedes striatal projection neuron pathology in heterozygous Q140 Huntington's disease mice. *Neurobiol Dis* 60:89–107
58. Lei W, Deng Y, Liu B et al (2013) Confocal laser scanning microscopy and ultrastructural study of VGLUT2 thalamic input to striatal projection neurons in rats. *J Comp Neurol* 521:1354–1377
59. Chen S, Yang G, Zhu Y et al (2016) A comparative study of three interneuron types in the rat spinal cord. *PLoS One* 11:e162969
60. Reiner A, Hart NM, Lei W et al (2010) Corticostriatal projection neurons—dichotomous types and dichotomous functions. *Front Neuroanat* 4:142
61. Liu B, Ouyang L, Mu S et al (2011) The morphological characteristics of corticostriatal and thalamostriatal neurons and their intrastriatal terminals in rats. *Surg Radiol Anat* 33:807–817
62. Gittis AH, Nelson AB, Thwin MT et al (2010) Distinct roles of GABAergic interneurons in the regulation of striatal output pathways. *J Neurosci* 30:2223–2234
63. Gustafson N, Gireesh-Dharmaraj E, Czubyko U et al (2006) A comparative voltage and current-clamp analysis of feedback and feedforward synaptic transmission in the striatal microcircuit in vitro. *J Neurophysiol* 95:737–752
64. Doig NM, Moss J, Bolam JP (2010) Cortical and thalamic innervation of direct and indirect pathway medium-sized spiny neurons in mouse striatum. *J Neurosci* 30:14610–14618
65. Goldberg JH, Tamas G, Yuste R (2003) Ca²⁺ imaging of mouse neocortical interneurone dendrites: Ia-type K⁺ channels control action potential backpropagation. *J Physiol* 551:49–65
66. Eggermann E, Jonas P (2011) How the “slow” Ca²⁺ buffer parvalbumin affects transmitter release in nanodomain-coupling regimes. *Nat Neurosci* 15:20–22
67. Aponte Y, Bischofberger J, Jonas P (2008) Efficient Ca²⁺ buffering in fast-spiking basket cells of rat hippocampus. *J Physiol* 586:2061–2075
68. Assous M, Tepper JM (2018) Excitatory extrinsic afferents to striatal interneurons and interactions with striatal microcircuitry. *Eur J Neurosci* 49(5):593–603
69. Day M, Wang Z, Ding J et al (2006) Selective elimination of glutamatergic synapses on striatopallidal neurons in Parkinson disease models. *Nat Neurosci* 9:251–259
70. Parker PR, Lalive AL, Kreitzer AC (2016) Pathway-specific remodeling of thalamostriatal synapses in parkinsonian mice. *Neuron* 89:734–740
71. Calabresi P, Pisani A, Mercuri NB et al (1996) The corticostriatal projection: from synaptic plasticity to dysfunctions of the basal ganglia. *Trends Neurosci* 19:19–24
72. Somogyi P (1977) A specific “axo-axonal” interneuron in the visual cortex of the rat. *Brain Res* 136:345–350
73. Woo TU, Whitehead RE, Melchitzky DS et al (1998) A subclass of prefrontal gamma-aminobutyric acid axon terminals are selectively altered in schizophrenia. *Proc Natl Acad Sci USA* 95:5341–5346
74. Liu B (2011) Morphological characteristics of the striatal neural pathway by biotinylated dextran amine tracing in. *Neural Regen Res* 6:1931–1936
75. Fujiyama F, Unzai T, Nakamura K et al (2006) Difference in organization of corticostriatal and thalamostriatal synapses between patch and matrix compartments of rat neostriatum. *Eur J Neurosci* 24:2813–2824

Publisher's Note Springer Nature remains neutral with regard to jurisdictional claims in published maps and institutional affiliations.